

1 **Search for spectral irregularities due to photon-axion-like particle**
2 **oscillations with the *Fermi* Large Area Telescope**

3 M. Ajello,¹ A. Albert,² B. Anderson,^{3,4} L. Baldini,^{5,2} G. Barbiellini,^{6,7} D. Bastieri,^{8,9}
4 R. Bellazzini,¹⁰ E. Bissaldi,¹¹ R. D. Blandford,² E. D. Bloom,² R. Bonino,^{12,13}
5 E. Bottacini,² J. Bregeon,¹⁴ P. Bruel,¹⁵ R. Buehler,¹⁶ G. A. Caliandro,^{2,17} R. A. Cameron,²
6 M. Caragiulo,^{18,11} P. A. Caraveo,¹⁹ C. Cecchi,^{20,21} A. Chekhtman,²² S. Ciprini,^{23,20}
7 J. Cohen-Tanugi,¹⁴ J. Conrad,^{3,4,24,*} F. Costanza,¹¹ F. D'Ammando,^{25,26} A. de Angelis,²⁷
8 F. de Palma,^{11,28} R. Desiante,^{29,12} M. Di Mauro,² L. Di Venere,^{18,11} A. Domínguez,¹
9 P. S. Drell,² C. Favuzzi,^{18,11} W. B. Focke,² A. Franckowiak,² Y. Fukazawa,³⁰ S. Funk,³¹
10 P. Fusco,^{18,11} F. Gargano,¹¹ D. Gasparrini,^{23,20} N. Giglietto,^{18,11} T. Glanzman,²
11 G. Godfrey,² S. Guiriec,^{32,33} D. Horan,¹⁵ G. Jóhannesson,³⁴ M. Katsuragawa,³⁵
12 S. Kensei,³⁰ M. Kuss,¹⁰ S. Larsson,^{36,4} L. Latronico,¹² J. Li,³⁷ L. Li,^{36,4} F. Longo,^{6,7}
13 F. Loparco,^{18,11} P. Lubrano,²⁰ G. M. Madejski,² S. Maldera,¹² A. Manfreda,¹⁰
14 M. Mayer,¹⁶ M. N. Mazziotta,¹¹ M. Meyer,^{3,4,†} P. F. Michelson,² N. Mirabal,^{32,33}
15 T. Mizuno,³⁸ M. E. Monzani,² A. Morselli,³⁹ I. V. Moskalenko,² S. Murgia,⁴⁰
16 M. Negro,^{12,13} E. Nuss,¹⁴ C. Okada,³⁰ E. Orlando,² J. F. Ormes,⁴¹ D. Paneque,^{42,2}
17 J. S. Perkins,³² M. Pesce-Rollins,^{10,2} F. Piron,¹⁴ G. Pivato,¹⁰ T. A. Porter,²
18 S. Rainò,^{18,11} R. Rando,^{8,9} M. Razzano,^{10,43} A. Reimer,^{44,2} M. Sánchez-Conde,^{4,3,‡}
19 C. Sgrò,¹⁰ D. Simone,¹¹ E. J. Siskind,⁴⁵ F. Spada,¹⁰ G. Spandre,¹⁰ P. Spinelli,^{18,11}
20 H. Takahashi,³⁰ J. B. Thayer,² D. F. Torres,^{37,46} G. Tosti,^{20,21} E. Troja,^{32,47}
21 Y. Uchiyama,⁴⁸ K. S. Wood,⁴⁹ M. Wood,² G. Zaharijas,^{50,51} and S. Zimmer^{3,4}

22 ¹*Department of Physics and Astronomy, Clemson University,*

23 *Kinard Lab of Physics, Clemson, SC 29634-0978, USA*

24 ²*W. W. Hansen Experimental Physics Laboratory,*

25 *Kavli Institute for Particle Astrophysics and Cosmology,*

26 *Department of Physics and SLAC National Accelerator Laboratory,*

27 *Stanford University, Stanford, CA 94305, USA*

28 ³*Department of Physics, Stockholm University,*

29 *AlbaNova, SE-106 91 Stockholm, Sweden*

30 ⁴*The Oskar Klein Centre for Cosmoparticle Physics,*

- 31 *AlbaNova, SE-106 91 Stockholm, Sweden*
- 32 ⁵*Università di Pisa and Istituto Nazionale di Fisica Nucleare,*
33 *Sezione di Pisa I-56127 Pisa, Italy*
- 34 ⁶*Istituto Nazionale di Fisica Nucleare,*
35 *Sezione di Trieste, I-34127 Trieste, Italy*
- 36 ⁷*Dipartimento di Fisica, Università di Trieste, I-34127 Trieste, Italy*
- 37 ⁸*Istituto Nazionale di Fisica Nucleare,*
38 *Sezione di Padova, I-35131 Padova, Italy*
- 39 ⁹*Dipartimento di Fisica e Astronomia “G. Galilei”,*
40 *Università di Padova, I-35131 Padova, Italy*
- 41 ¹⁰*Istituto Nazionale di Fisica Nucleare,*
42 *Sezione di Pisa, I-56127 Pisa, Italy*
- 43 ¹¹*Istituto Nazionale di Fisica Nucleare,*
44 *Sezione di Bari, I-70126 Bari, Italy*
- 45 ¹²*Istituto Nazionale di Fisica Nucleare,*
46 *Sezione di Torino, I-10125 Torino, Italy*
- 47 ¹³*Dipartimento di Fisica Generale “Amadeo Avogadro” ,*
48 *Università degli Studi di Torino, I-10125 Torino, Italy*
- 49 ¹⁴*Laboratoire Univers et Particules de Montpellier,*
50 *Université Montpellier, CNRS/IN2P3, Montpellier, France*
- 51 ¹⁵*Laboratoire Leprince-Ringuet, École polytechnique, CNRS/IN2P3, Palaiseau, France*
- 52 ¹⁶*Deutsches Elektronen Synchrotron DESY, D-15738 Zeuthen, Germany*
- 53 ¹⁷*Consorzio Interuniversitario per la Fisica Spaziale (CIFS), I-10133 Torino, Italy*
- 54 ¹⁸*Dipartimento di Fisica “M. Merlin” dell’Università*
55 *e del Politecnico di Bari, I-70126 Bari, Italy*
- 56 ¹⁹*INAF-Istituto di Astrofisica Spaziale e Fisica Cosmica, I-20133 Milano, Italy*
- 57 ²⁰*Istituto Nazionale di Fisica Nucleare,*
58 *Sezione di Perugia, I-06123 Perugia, Italy*
- 59 ²¹*Dipartimento di Fisica, Università degli Studi di Perugia, I-06123 Perugia, Italy*
- 60 ²²*College of Science, George Mason University, Fairfax, VA 22030,*
61 *resident at Naval Research Laboratory, Washington, DC 20375, USA*
- 62 ²³*Agenzia Spaziale Italiana (ASI) Science Data Center, I-00133 Roma, Italy*

63
64
65
66
67
68
69
70
71
72
73
74
75
76
77
78
79
80
81
82
83
84
85
86
87
88
89
90
91
92
93

²⁴Wallenberg Academy Fellow

²⁵INAF Istituto di Radioastronomia, I-40129 Bologna, Italy

²⁶Dipartimento di Astronomia, Università di Bologna, I-40127 Bologna, Italy

²⁷Dipartimento di Fisica, Università di Udine and Istituto Nazionale di Fisica Nucleare,
Sezione di Trieste, Gruppo Collegato di Udine, I-33100 Udine

²⁸Università Telematica Pegaso, Piazza Trieste e Trento, 48, I-80132 Napoli, Italy

²⁹Università di Udine, I-33100 Udine, Italy

³⁰Department of Physical Sciences, Hiroshima University,

Higashi-Hiroshima, Hiroshima 739-8526, Japan

³¹Erlangen Centre for Astroparticle Physics, D-91058 Erlangen, Germany

³²NASA Goddard Space Flight Center, Greenbelt, MD 20771, USA

³³NASA Postdoctoral Program Fellow, USA

³⁴Science Institute, University of Iceland, IS-107 Reykjavik, Iceland

³⁵Institute of Space and Astronautical Science,

Japan Aerospace Exploration Agency, 3-1-1 Yoshinodai,

Chuo-ku, Sagami-hara, Kanagawa 252-5210, Japan

³⁶Department of Physics, KTH Royal Institute of Technology,

AlbaNova, SE-106 91 Stockholm, Sweden

³⁷Institute of Space Sciences (IEEC-CSIC),

Campus UAB, E-08193 Barcelona, Spain

³⁸Hiroshima Astrophysical Science Center, Hiroshima University,

Higashi-Hiroshima, Hiroshima 739-8526, Japan

³⁹Istituto Nazionale di Fisica Nucleare,

Sezione di Roma "Tor Vergata", I-00133 Roma, Italy

⁴⁰Center for Cosmology, Physics and Astronomy Department,

University of California, Irvine, CA 92697-2575, USA

⁴¹Department of Physics and Astronomy,

University of Denver, Denver, CO 80208, USA

⁴²Max-Planck-Institut für Physik, D-80805 München, Germany

⁴³Funded by contract FIRB-2012-RBFR12PM1F from the
Italian Ministry of Education, University and Research (MIUR)

94 ⁴⁴*Institut für Astro- und Teilchenphysik and Institut für Theoretische Physik,*
95 *Leopold-Franzens-Universität Innsbruck, A-6020 Innsbruck, Austria*

96 ⁴⁵*NYCB Real-Time Computing Inc.,*
97 *Lattintown, NY 11560-1025, USA*

98 ⁴⁶*Institució Catalana de Recerca i Estudis Avançats (ICREA), Barcelona, Spain*

99 ⁴⁷*Department of Physics and Department of Astronomy,*
100 *University of Maryland, College Park, MD 20742, USA*

101 ⁴⁸*Department of Physics, 3-34-1 Nishi-Ikebukuro,*
102 *Toshima-ku, Tokyo 171-8501, Japan*

103 ⁴⁹*Space Science Division, Naval Research Laboratory, Washington, DC 20375-5352, USA*

104 ⁵⁰*Istituto Nazionale di Fisica Nucleare, Sezione di Trieste,*
105 *and Università di Trieste, I-34127 Trieste, Italy*

106 ⁵¹*Laboratory for Astroparticle Physics, University of Nova Gorica,*
107 *Vipavska 13, SI-5000 Nova Gorica, Slovenia*

108 (Dated: April 6, 2016)

Abstract

We report on the search for spectral irregularities induced by oscillations between photons and axion-like particles (ALPs) in the γ -ray spectrum of NGC 1275, the central galaxy of the Perseus cluster. Using six years of *Fermi* Large Area Telescope data, we find no evidence for ALPs and exclude couplings above $5 \times 10^{-12} \text{ GeV}^{-1}$ for ALP masses $0.5 \lesssim m_a \lesssim 5 \text{ neV}$ at 95% confidence. The limits are competitive with the sensitivity of planned laboratory experiments, and, together with other bounds, strongly constrain the possibility that ALPs can reduce the γ -ray opacity of the Universe.

109 INTRODUCTION

110 Axions and axion-like particles (ALPs) are predicted by a variety of extensions of the
111 Standard Model [1–6]. If produced non-thermally in the early Universe, these particles may
112 account for all or a significant fraction of the cold dark matter (DM) [e.g. 7–9], and could
113 be detected through their coupling to photons in magnetic fields [10]. While the axion mass
114 is proportional to its coupling to photons, these two parameters are independent in the case
115 of ALPs.

116 Photon-ALP interactions could leave an imprint on γ -ray spectra, provided that the
117 ALP mass is sufficiently small, $m_a \lesssim \mu\text{eV}$. Above a critical energy E_{crit} photon-ALP mixing
118 becomes maximal, leading to a reduction of the photon flux [11, 12]. Around E_{crit} this is
119 accompanied by spectral irregularities that depend on the strength and morphology of the
120 magnetic field [13]. Photon-ALP conversions could also reduce the opacity of the Universe
121 caused by pair production of γ rays with photons of the extragalactic background light
122 (EBL) [14]. Evidence exists that the γ -ray absorption is indeed lower than expected from
123 state-of-the-art EBL models [15–18], and ALPs have been used to explain these observations
124 [19–22] (see, however, [23, 24]).

125 Sources embedded in galaxy clusters are promising to search for ALPs due to the strong
126 magnetic fields extending over large spatial scales in these systems. For example, the absence
127 of irregularities above 200 GeV in the spectrum of the blazar PKS 2155-304, associated with
128 a poor galaxy cluster, has been used to constrain the photon-ALP coupling [25]. Here, we
129 focus on the search for irregularities in the spectrum of the radio galaxy NGC 1275 with
130 the *Fermi* Large Area Telescope (LAT). NGC 1275 is the most favorable target since it is
131 a bright γ -ray emitter detected with a significance exceeding 100σ in the third *Fermi*-LAT
132 source catalog (3FGL) [26]. Its broadband emission can be explained with synchrotron-self
133 Compton models, which predict a smooth γ -ray spectrum [28, 29]. It is located at the center
134 of the Perseus cool-core cluster for which rotation measures (RMs) suggest a high central
135 magnetic field [30].

136 Our analysis makes use of the newest **Pass 8** event-level analysis for LAT data. Compared
137 to previous Passes, **Pass 8** has an improved angular resolution, a broader energy range,
138 larger effective area, as well as reduced uncertainties in the instrumental response functions
139 (IRFs) [31].

140 LAT DATA SELECTION

141 We make use of six years of LAT data taken between 2008-08-04 and 2014-08-04 in the
142 energy range from 100 MeV to 500 GeV. For lower energies, the effective area decreases
143 rapidly and the energy dispersion increases. At energies above 500 GeV we do not expect
144 sufficient photon statistics [32]. We only consider events that arrive at a zenith angle $\theta_z < 90^\circ$
145 in order to minimize the contribution of γ rays from the Earth limb. Time intervals that
146 correspond to bright solar flares and γ -ray bursts are excluded. We extract γ -ray like
147 events within a $10^\circ \times 10^\circ$ region of interest (ROI) centered at the position of NGC 1275:
148 $\alpha_{2000} = 3^{\text{h}}19^{\text{m}}49.9^{\text{s}}$, $\delta_{2000} = +41^\circ30^{\text{m}}49.2^{\text{s}}$ [26].

149 Events passing the `Pass 8 P8R2_SOURCE` selection cuts are analyzed using the `P8R2_SOURCE_V6`
150 IRFs.¹ An innovation of the `Pass 8` IRFs is the possibility to subdivide an event class into
151 event types according to the quality of the angular or energy reconstruction (PSF and
152 EDISP event types, respectively). In this analysis we will use the EDISP types to maximize
153 our sensitivity to spectral irregularities. Events are classified into one of four types ranging
154 from EDISP0 to EDISP3, that denote the quality of the energy reconstruction from worst to
155 best. All EDISP event types have a similar number of events in each logarithmic energy bin
156 and are mutually exclusive. The energy dispersion matrices are given in the Supplemental
157 Material [27].

158 PHOTON-ALP OSCILLATIONS

159 Following [16, 33, 34], we derive the probability $P_{\gamma\gamma}$ for a final state photon in the photon-
160 ALP beam as a function of energy for an initially un-polarized photon beam (see the Sup-
161 plemental Material). We expect the irregularities to occur around a critical energy [35],

$$E_{\text{crit}} \sim 2.5 \text{ GeV} \frac{|m_{a,\text{neV}}^2 - \omega_{\text{pl,neV}}^2|}{g_{11} B_{\mu\text{G}}}, \quad (1)$$

162 with ALP mass $m_{a,\text{neV}}$ and plasma frequency $\omega_{\text{pl,neV}}$ in units of neV, coupling constant
163 $g_{11} = g_{a\gamma}/10^{-11}\text{GeV}^{-1}$, and magnetic field $B_{\mu\text{G}} = B/1 \mu\text{G}$. We include photon-ALP mixing
164 in the intra-cluster and Galactic magnetic fields. The B field of the Milky Way is modeled
165 with the coherent component of the model described in [36]. We do not include its turbulent

¹ http://www.slac.stanford.edu/exp/glast/groups/canda/lat_Performance.htm

166 component, as the scales on which the turbulence occurs are usually smaller than the photon-
 167 ALP oscillation length. The turbulent intra-cluster B field is described below. Absorption
 168 of γ rays by the EBL is taken into account through the model of [37]. We neglect any
 169 oscillations in the intergalactic magnetic field (IGMF). With current upper limits on the
 170 IGMF strength of $\lesssim 10^{-9}$ G and on the photon-ALP coupling, $g_{11} < 6.6$ [38], we find that
 171 $E_{\text{crit}} \lesssim 100$ GeV only for $m_{a,\text{neV}} \lesssim 0.5$. For such low masses, g_{11} is further constrained below
 172 0.6 from the non-observation of γ rays from SN1987A [39]. Given this small coupling and the
 173 comparatively short distance to NGC 1275 (redshift $z = 0.017559$), no strong irregularities
 174 should be induced by mixing in the IGMF.

175 **Intra-cluster magnetic field**

176 Faraday RM observations and magneto-hydrodynamic simulations suggest that the mag-
 177 netic field in galaxy clusters is turbulent and that its strength follows the electron density
 178 $n_e(r)$ of the intra-cluster medium (ICM), $B(r) = B_0(n_e(r)/n_e(r=0))^\eta$ [40–42]. We model
 179 the turbulent component as a divergence-free homogeneous isotropic field with Gaussian
 180 turbulence with zero mean and a variance σ_B [34]. The energy density follows a power law
 181 $M(k) \propto k^q$ in wave numbers k . It is non-zero only between the minimum and maximum
 182 turbulence scales $k_L = 2\pi/\Lambda_{\text{max}}$ and $k_H = 2\pi/\Lambda_{\text{min}}$.

183 For the Perseus cluster, we use $n_e(r)$ derived from X-ray observations (Eq. (4) in [43])
 184 within the inner $r_{\text{max}} = 500$ kpc. Beyond this radius, we conservatively assume a zero mag-
 185 netic field. RMs currently only probe the innermost region (tens of pc) around NGC 1275.
 186 The observations lead to an estimated central magnetic field of $25 \mu\text{G}$ [30]. An independent
 187 lower limit of $B_0 \gtrsim 2\text{--}13 \mu\text{G}$ for $0.3 \leq \eta \leq 0.7$ has been derived from MAGIC observations
 188 of the Perseus cluster [44]. These results motivate our assumptions for $\sigma_B = 10 \mu\text{G}$ and
 189 $\eta = 0.5$, which are also in line with observations of other cool-core clusters [e.g. 45, 46].

190 For the turbulence spectrum, we assume values derived from RMs of the cool-core cluster
 191 A 2199 [46], which has a comparable number of member galaxies. The fiducial parameter
 192 choices are summarized in Tab. I.

Parameter	Value
σ_B	10 μ G
r_{\max}	500 kpc
η	0.5
q	-2.8
Λ_{\min}	0.7 kpc
Λ_{\max}	35 kpc

TABLE I. Fiducial model parameters for the intra-cluster magnetic field in Perseus.

193 DATA ANALYSIS

194 We perform a binned Poisson likelihood analysis, similar to the DM signal search from
 195 dwarf spheroidal galaxies [47, 48]. Events are binned into $10^\circ \times 10^\circ$ sky maps with a resolution
 196 of 0.2° per pixel. The width of the logarithmically spaced energy bins is chosen to be 30 %
 197 of the median energy resolution of each EDISP event type (see the Supplemental Material
 198 for details). This results in 39, 67, 94, and 145 energy bins for EDISP0-3, respectively. We
 199 have tested with simulations that bin sizes below 40 % of the median energy resolution do
 200 not affect the results.

201 For each event type, we perform a fit over the entire energy range and ROI for all source
 202 parameters (nuisance parameters θ_i) using *gtlike* included in the *Fermi-LAT Science Tools*
 203 version v10r01p01.² We include all point sources listed in the 3FGL within 15° from the
 204 ROI center. The diffuse backgrounds are modeled with templates for the Galactic and
 205 the isotropic extragalactic γ -ray emission.³ The energy dispersion is taken into account in
 206 the fitting of the point sources whereas it is already accounted for in the the data-driven
 207 derivation of the diffuse templates. Normalizations of the diffuse sources and point sources
 208 within 8° from the ROI center are left free to vary. All spectral indices of the point sources
 209 within 4° are also free parameters. The time-averaged spectrum of NGC 1275 is modeled
 210 with a logarithmic (log) parabola, $F(E) = N(E/E_0)^{-(\alpha+\beta \ln(E/E_0))}$, where E_0 is fixed to
 211 530 MeV [26].

212 Under the assumption that the profiled nuisance parameters do not change when con-

² <http://fermi.gsfc.nasa.gov/ssc/data/analysis/>

³ <http://fermi.gsfc.nasa.gov/ssc/data/access/lat/BackgroundModels.html>

213 sidering each bin separately [47], we extract the likelihood in each reconstructed energy bin
 214 k' , $\mathcal{L}(\mu_{ik'}, \boldsymbol{\theta}_i | D_{ik'})$ as a function of expected counts $\mu_{ik'}$ of NGC 1275, and observed counts
 215 $D_{ik'}$. For NGC 1275 a power law with fixed spectral index $\Gamma = 2$ is now assumed in each
 216 bin. For each tested value of $\mu_{ik'}$ we re-optimize the normalization of the spectrum of the
 217 radio galaxy IC 310 which has an angular separation of $\sim 0.6^\circ$ from NGC 1275.

218 Under the ALP hypothesis, characterized by $P_{\gamma\gamma} \equiv P_{\gamma\gamma}(E, m_a, g_{a\gamma}, \mathbf{B}_j)$ for one random
 219 turbulent B -field realization \mathbf{B}_j , the expected number of photons is calculated through

$$\mu_{ik'} = \sum_k \mathcal{D}_{kk'}^i \int_{\Delta E_k} dE P_{\gamma\gamma} F(E) \mathcal{E}^i(E), \quad (2)$$

220 where the integration runs over the true energy bin ΔE_k , \mathcal{E}^i is the exposure, and $\mathcal{D}_{kk'}^i$ is
 221 the energy dispersion for event type EDISP*i*. Under the null hypothesis, $P_{\gamma\gamma}$ reduces to
 222 the EBL attenuation. The parameters of the intrinsic source spectrum $F(E)$, N , α , and β ,
 223 are further nuisance parameters. For each tested ALP parameter and magnetic field, we
 224 determine these parameters by profiling the joint likelihood of all energy bins k'

$$\mathcal{L}_i(\boldsymbol{\mu}, \boldsymbol{\theta} | \mathbf{D}) \equiv \prod_{k'} \mathcal{L}(\mu_{ik'}, \boldsymbol{\theta}_i | D_{ik'}), \quad (3)$$

225 for each event type separately, using the pre-computed likelihood curves $\mathcal{L}(\mu_{ik'}, \boldsymbol{\theta}_i | D_{ik'})$. In
 226 this way, we treat each event type selection as an independent measurement.⁴ The bin-
 227 by-bin likelihood curves for the EDISP3 event type are shown in Fig. 1 together with the
 228 best-fit spectra.

229 We simulate $N_B = 500$ random realizations of the turbulent field \mathbf{B}_j , $j = 1, \dots, N_B$. The
 230 dependence of the likelihood on the realizations is not easily parametrizable and we cannot
 231 assume that the simulations map the space of possible realizations. Therefore, instead of
 232 profiling, we sort the B -field realizations for each tested $(m_a, g_{a\gamma})$ pair by increasing values of
 233 the product over the likelihoods \mathcal{L}_i and use the realization that corresponds to the $Q_B = 0.95$
 234 quantile of the likelihood distribution (profiling would correspond to $Q_B = 1$). We will
 235 denote this realization as \mathbf{B}_{95} and the corresponding expected counts with $\boldsymbol{\mu}_{95}$. Note that
 236 \mathbf{B}_{95} might be different for different ALP parameters, so that $\mathbf{B}_{95} \equiv \mathbf{B}_{95}(m_a, g_{a\gamma})$.

⁴ This procedure will result in different best-fit estimators for the source parameters for each event type.

In this way, it is possible to speed up the optimization considerably. We have verified that our results do not change when the parameters of NGC 1275 are tied over the event types.

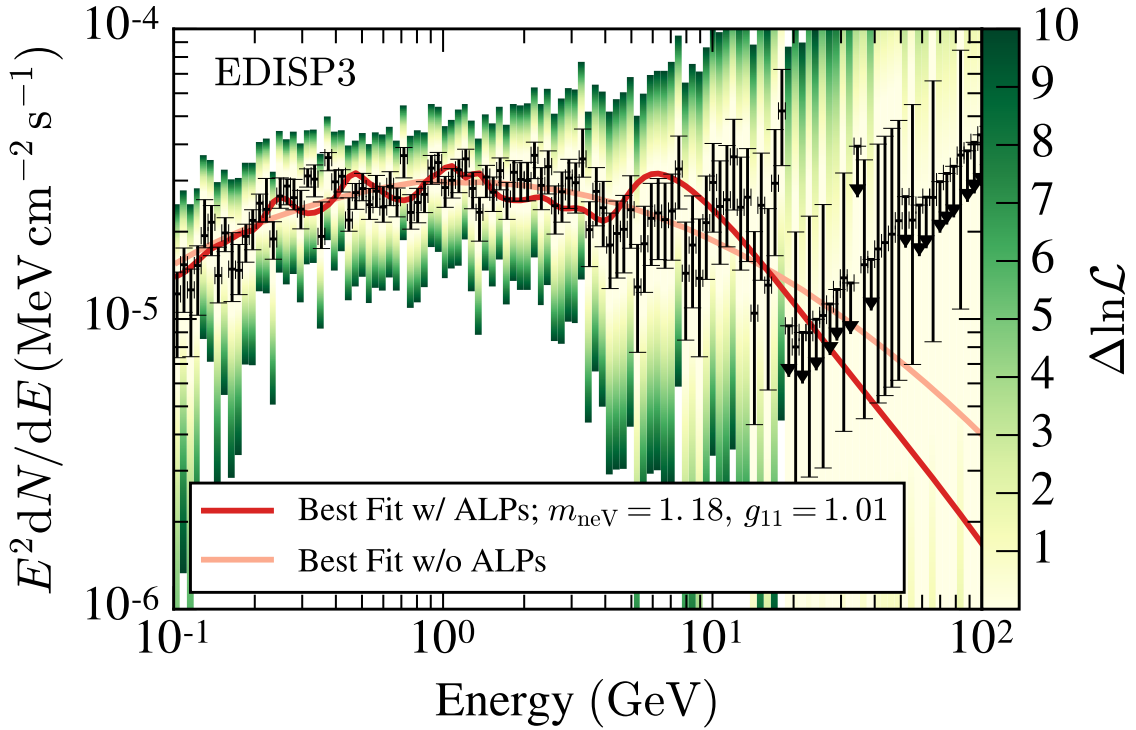


FIG. 1. The likelihood curves (shown in color) for the EDISP3 event type. $\Delta \ln \mathcal{L} = 0$ corresponds to the maximum likelihood in each bin (black points). The error bars indicate an increase of the likelihood by $2\Delta \ln \mathcal{L} = 1$. The best-fit spectrum of the joint likelihood without an ALP (with an ALP with $m_{\text{neV}} = 1.2$ and $g_{11} = 1$) is shown as a light (dark) red solid line.

237 Similar to [49], we evaluate the ALP hypothesis with a likelihood ratio test. The test
 238 statistic (TS) for the ALP hypothesis is calculated from the joint likelihood of all event
 239 types:

$$\text{TS} = -2 \sum_i \ln \left(\frac{\mathcal{L}_i(\boldsymbol{\mu}_0, \hat{\boldsymbol{\theta}}|\mathbf{D})}{\mathcal{L}_i(\hat{\boldsymbol{\mu}}_{95}, \hat{\boldsymbol{\theta}}|\mathbf{D})} \right), \quad (4)$$

240 where $\boldsymbol{\mu}_0$ are the expected counts for the null (no ALP) hypothesis with maximized nuisance
 241 parameters $\hat{\boldsymbol{\theta}} \equiv \hat{\boldsymbol{\theta}}(\boldsymbol{\mu}_0)$ and $\hat{\boldsymbol{\mu}}_{95}$ are the expected counts under the ALP hypothesis that,
 242 together with $\hat{\boldsymbol{\theta}}$, maximize the likelihoods of each event type. We test ALP parameters on a
 243 logarithmic $(m_a, g_{a\gamma})$ grid with (19×12) steps where $0.07 \leq m_{a,\text{neV}} \leq 100$ and $0.1 \leq g_{11} \leq 7$.
 244 The mass range is chosen such that E_{crit} falls into the analyzed energy range whereas the
 245 maximum coupling is motivated by the bound found in [38]. For the lower bound, the

246 amplitude of the irregularities is too small to be detectable.

247 In order to convert the TS value into a significance, we need to know the underlying
248 probability distribution. We derive the null distribution from Monte-Carlo simulations and
249 from it the threshold TS value, TS_{thr} , for which we can reject the null hypothesis (see the
250 Supplemental Material for details). For a rejection of the no-ALP hypothesis at a 3σ (global)
251 significance level, we find that $\text{TS} > \text{TS}_{\text{thr}} = 33.1$.

252 RESULTS

253 The best-fit ALP parameters are found at $m_{\text{neV}} = 44.6$ and $g_{11} = 4.76$ with $\text{TS} =$
254 $10.40 < \text{TS}_{\text{thr}}$, and hence the best fit with ALPs is not significantly preferred over the null
255 hypothesis. We set upper limits by stepping over the ALP parameters and calculating the
256 difference $\lambda(m_a, g_{a\gamma})$ between the log-likelihood values for each pair $m_a, g_{a\gamma}$ and the best fit.
257 ALP parameters are excluded with 95% confidence if $\lambda > \lambda_{\text{thr}} = 22.8$. The threshold value
258 λ_{thr} is calculated under the assumption that the probability distribution of the alternative
259 hypothesis follows the null distribution. We have tested this assumption with simulations
260 and found that this choice results in over coverage for ALP parameters causing the strongest
261 irregularities, thus yielding conservative limits.

262 The excluded parameter space is shown in the left panel of Fig. 2 (black shaded region).
263 Photon-ALP couplings are ruled out between $0.5 \lesssim g_{11} \lesssim 3$ for $0.5 \lesssim m_{a,\text{neV}} \lesssim 5$ and $g_{11} \gtrsim 1$
264 for $5 \lesssim m_{a,\text{neV}} \lesssim 10$. At high masses, the limits run almost parallel to the lines of constant
265 E_{crit} (shown as dotted lines for $B_{\mu\text{G}} = 10$). For lower masses, ALP couplings along the
266 $E_{\text{crit}} = 1\text{ GeV}$ line with $1.3 \lesssim g_{11} \lesssim 4$ are not excluded. Around this “hole”-like feature,
267 $P_{\gamma\gamma}$ exhibits rapid fluctuations for almost the entire *Fermi*-LAT energy range. Given the
268 Poisson noise in the data, these ALP parameters cannot be excluded. We stress that the
269 fit with ALPs is not preferred over the null hypothesis. For masses below $m_{a,\text{neV}} = 0.5$,
270 irregularities still enter the *Fermi*-LAT energy range allowing to exclude ALP parameters.

271 The observed limits agree well with the expected exclusion region derived from Monte-
272 Carlo simulations (shaded regions). The “hole” feature is not visible in the expected limits
273 but occurs in certain Monte-Carlo realizations (an example is given in the Supplemental
274 Material). In 5% of the simulations (yellow shaded region), ALP parameters are excluded
275 for which the $E_{\text{crit}} > 100\text{ GeV}$. This is expected since we have derived λ_{thr} from the null

276 distribution where for 5 % of the simulations one finds $\text{TS} > \lambda_{\text{thr}}$. The parameters for which
 277 we could detect an ALP signal at a 2σ level agree well with the observed limits (gray hatched
 278 region; see the Supplemental Material for details).

279 The results are subject to systematic uncertainties related to the analysis and magnetic
 280 field parameters. Concerning the analysis, changing the energy dispersion has the strongest
 281 effect on the limits. If we conservatively broaden the energy dispersion by 20 % the area of
 282 the tested ALP parameter grid with $\lambda > 22.8$ decreases by 25 %. All other tested effects
 283 related to the analysis change the limits at most by $\sim 4\%$. Concerning the choice of
 284 B -field parameters, neither the strength, the power spectrum, nor the dependence on the
 285 electron density of the magnetic field are well established for Perseus. Therefore, the full
 286 analysis is repeated for a magnetic-field strength of $\sigma_B = 20\ \mu\text{G}$, for a Kolmogorov-type
 287 turbulence spectrum, $q = -11/3$ (as found in the cool-core cluster Hydra A, [e.g. 45]), and
 288 by conservatively assuming that the magnetic field is zero beyond $r_{\text{max}} = 100\ \text{kpc}$. Increasing
 289 σ_B increases the excluded area by 43 %. In comparison, the other tested parameters have a
 290 subdominant effect of maximally 16 %. The dependence of the limits on the particular choice
 291 of the EBL model is negligible due to the relative proximity of NGC 1275 ($z = 0.017559$).
 292 The absorption is maximally $\sim 8\%$ at 500 GeV with significantly smaller relative differences
 293 for a number of EBL models [37, 50–54]. We provide a comprehensive summary of all tested
 294 systematic uncertainties in the Supplemental Material.

295 The limits derived in this work are compared to other limits and sensitivities of future
 296 experiments in Fig. 2 (right). Our results give the strongest constraints to date for $0.5 \lesssim$
 297 $m_{a,\text{neV}} \lesssim 20$ and surpass the expected limits for the planned ALPS II experiment [55] in that
 298 range. They are only a factor of ~ 2 below the exclusion prospects of the planned IAXO
 299 experiment [56]. We note that the systematic uncertainties of the future experiments are
 300 likely to be smaller than the ones that apply to the present analysis. In conjunction with
 301 other limits taken at face value [25, 39, 49], the parameter space where ALPs could explain
 302 hints for a lower γ -ray opacity compared to EBL-model predictions (light blue region, [21])
 303 is now strongly constrained. The limits do not constrain ALPs that could make up the
 304 entire DM content of the Universe. This corresponds to the region in Fig. 2 (right) below
 305 the $\theta_1 \mathcal{N} = 1$ line, where \mathcal{N} is a model dependent factor and θ_1 is the misalignment angle [9].
 306 Our analysis only constrains ALPs that make up less than 4 % of the DM, or equivalently
 307 $\theta_1 \mathcal{N} > 5$.

308 Observations with future γ -ray instruments could improve the reported limits and test
 309 ALP DM models. The planned Gamma-400 satellite, with an envisaged energy resolution
 310 of 1% above 10 GeV [57], might be able to better resolve the spectra and probe higher ALP
 311 masses. Higher masses could also be reached with the future Cherenkov Telescope Array
 312 (CTA) [58].

313 It will be possible to reduce the uncertainties of the intra-cluster B field with the upcoming
 314 Square Kilometer Array (SKA) that will conduct a full-sky polarisation survey [59]. It is
 315 expected that SKA will observe hundreds of RMs of background sources for the most massive
 316 clusters, thereby enabling a more precise determination of their magnetic fields [60].

317 The analysis presented here can be easily extended to other sources that reside in clusters
 318 (e.g. M87 in the Virgo cluster) or in general to any source where ALP-induced spectral
 319 irregularities are expected. ALP parameters not constrained in the present analysis (such
 320 as those of the “hole”-like feature) could be probed with the different B -field configurations
 321 in other sources.

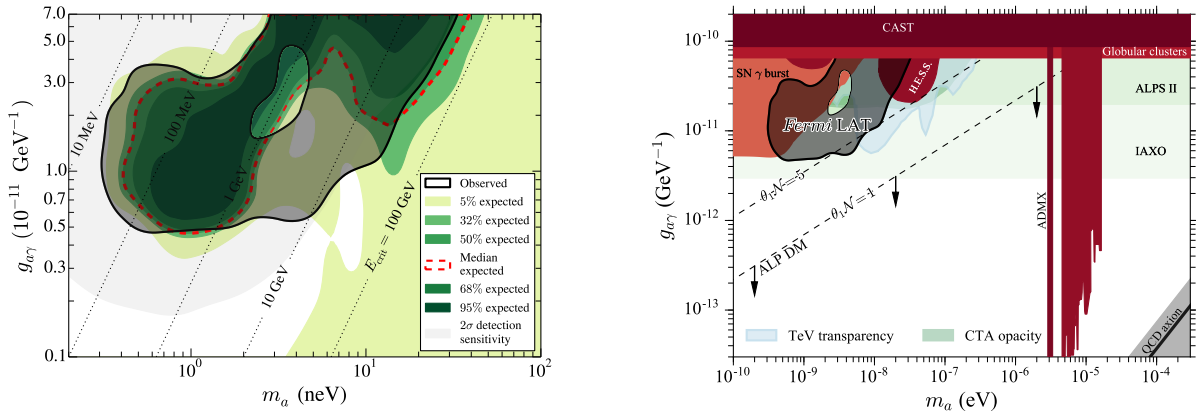


FIG. 2. *Left*: Observed and expected 95% confidence limits on the ALP parameters from 400 Monte-Carlo simulations. Dotted lines correspond to constant critical energies. The hatched gray region shows the parameters where ALPs are detectable at the 2σ confidence level (median sensitivity). *Right*: Comparison of *Fermi*-LAT limits with other works. Other Limits are shown in red, expected sensitivities in green. The parameter space where ALPs could explain a low γ -ray opacity is shown in blue. ALPs below the $\mathcal{N}\theta_1 = 1$ line could account for all the DM. The QCD axion is shown as a gray shaded band and solid black line. See, e.g. [61] and references therein.

322 **ACKNOWLEDGMENTS**

323 The *Fermi*-LAT Collaboration acknowledges support for LAT development, operation
324 and data analysis from NASA and DOE (United States), CEA/Irfu and IN2P3/CNRS
325 (France), ASI and INFN (Italy), MEXT, KEK, and JAXA (Japan), and the K.A. Wal-
326 lenberg Foundation, the Swedish Research Council and the National Space Board (Sweden).
327 Science analysis support in the operations phase from INAF (Italy) and CNES (France) is
328 also gratefully acknowledged.

329 * conrad@fysik.su.se

330 † manuel.meyer@fysik.su.se

331 ‡ sanchezconde@fysik.su.se

- 332 [1] J. Jaeckel and A. Ringwald, Annual Review of Nuclear and Particle Science **60**, 405 (2010),
333 arXiv:1002.0329 [hep-ph].
- 334 [2] R. D. Peccei and H. R. Quinn, Physical Review Letters **38**, 1440 (1977).
- 335 [3] S. Weinberg, Physical Review Letters **40**, 223 (1978).
- 336 [4] F. Wilczek, Physical Review Letters **40**, 279 (1978).
- 337 [5] E. Witten, Physics Letters B **149**, 351 (1984).
- 338 [6] A. Ringwald, Journal of Physics Conference Series **485**, 012013 (2014).
- 339 [7] J. Preskill, M. B. Wise, and F. Wilczek, Physics Letters B **120**, 127 (1983).
- 340 [8] D. J. E. Marsh, Phys. Rev. D **83**, 123526 (2011), arXiv:1102.4851 [astro-ph.CO].
- 341 [9] P. Arias, D. Cadamuro, M. Goodsell, J. Jaeckel, J. Redondo, and A. Ringwald, JCAP **6**, 013
342 (2012), arXiv:1201.5902 [hep-ph].
- 343 [10] G. Raffelt and L. Stodolsky, Phys. Rev. D **37**, 1237 (1988).
- 344 [11] K. A. Hochmuth and G. Sigl, Phys. Rev. D **76**, 123011 (2007), arXiv:0708.1144.
- 345 [12] A. de Angelis, O. Mansutti, and M. Roncadelli, Physics Letters B **659**, 847 (2008),
346 arXiv:0707.2695.
- 347 [13] D. Wouters and P. Brun, Phys. Rev. D **86**, 043005 (2012), arXiv:1205.6428 [astro-ph.HE].
- 348 [14] A. de Angelis, M. Roncadelli, and O. Mansutti, Phys. Rev. D **76**, 121301 (2007),
349 arXiv:0707.4312.

- 350 [15] A. De Angelis, O. Mansutti, M. Persic, and M. Roncadelli, MNRAS **394**, L21 (2009),
351 arXiv:0807.4246.
- 352 [16] A. de Angelis, G. Galanti, and M. Roncadelli, Phys. Rev. D **84**, 105030 (2011),
353 arXiv:1106.1132 [astro-ph.HE].
- 354 [17] D. Horns and M. Meyer, JCAP **2**, 033 (2012), arXiv:1201.4711 [astro-ph.CO].
- 355 [18] G. Rubtsov and S. Troitsky, JETP Lett. **100**, 397 (2014), arXiv:1406.0239 [astro-ph.HE].
- 356 [19] M. A. Sánchez-Conde, D. Paneque, E. Bloom, *et al.*, Phys. Rev. D **79**, 123511 (2009),
357 arXiv:0905.3270 [astro-ph.CO].
- 358 [20] A. Domínguez, M. A. Sánchez-Conde, and F. Prada, JCAP **11**, 020 (2011), arXiv:1106.1860
359 [astro-ph.CO].
- 360 [21] M. Meyer, D. Horns, and M. Raue, Phys. Rev. D **87**, 035027 (2013), arXiv:1302.1208 [astro-
361 ph.HE].
- 362 [22] G. Galanti, M. Roncadelli, A. De Angelis, and G. F. Bignami, ArXiv e-prints (2015),
363 arXiv:1503.04436 [astro-ph.HE].
- 364 [23] J. Biteau and D. A. Williams, ArXiv e-prints (2015), arXiv:1502.04166.
- 365 [24] A. Domínguez and M. Ajello, ApJ **813**, L34 (2015), arXiv:1510.07913 [astro-ph.HE].
- 366 [25] A. Abramowski, F. Acero, F. Aharonian, *et al.* (H.E.S.S. Collaboration), Phys. Rev. D **88**,
367 102003 (2013), arXiv:1311.3148 [astro-ph.HE].
- 368 [26] M. Ackermann *et al.* (*Fermi*-LAT Collaboration), Astrophys. J. **810**, 14 (2015),
369 arXiv:1501.06054 [astro-ph.HE].
- 370 [27] See Supplemental Material, which includes Refs. [62-72].
- 371 [28] J. Aleksić *et al.* (MAGIC Collaboration), A&A **564**, A5 (2014), arXiv:1310.8500 [astro-ph.HE].
- 372 [29] F. Tavecchio and G. Ghisellini, MNRAS **443**, 1224 (2014), arXiv:1404.6894 [astro-ph.HE].
- 373 [30] G. B. Taylor, N. E. Gugliucci, A. C. Fabian, *et al.*, MNRAS **368**, 1500 (2006), astro-
374 ph/0602622.
- 375 [31] W. Atwood, A. Albert, L. Baldini, *et al.*, ArXiv e-prints (2013), arXiv:1303.3514 [astro-
376 ph.IM].
- 377 [32] M. Ackermann *et al.* (*Fermi*-LAT Collaboration), Accepted for publication in ApJS (2015),
378 arXiv:1508.04449 [astro-ph.HE].
- 379 [33] C. Csáki, N. Kaloper, M. Peloso, and J. Terning, JCAP **5**, 005 (2003), hep-ph/0302030.
- 380 [34] M. Meyer, D. Montanino, and J. Conrad, JCAP **9**, 003 (2014), arXiv:1406.5972 [astro-ph.HE].

- 381 [35] D. Hooper and S. Profumo, *Phys. Rep.* **453**, 29 (2007), arXiv:hep-ph/0701197.
- 382 [36] R. Jansson and G. R. Farrar, *ApJ* **757**, 14 (2012), arXiv:1204.3662 [astro-ph.GA].
- 383 [37] A. Domínguez, J. R. Primack, D. J. Rosario, *et al.*, *MNRAS* **410**, 2556 (2011), arXiv:1007.1459
384 [astro-ph.CO].
- 385 [38] A. Ayala, I. Domínguez, M. Giannotti, *et al.*, *Phys. Rev. Lett.* **113**, 191302 (2014),
386 arXiv:1406.6053 [astro-ph.SR].
- 387 [39] A. Payez, C. Evoli, T. Fischer, *et al.*, *JCAP* **2**, 006 (2015), arXiv:1410.3747 [astro-ph.HE].
- 388 [40] K. Dolag, A. M. Bykov, and A. Diaferio, *Space Sci. Rev.* **134**, 311 (2008), arXiv:0801.1048.
- 389 [41] Y. Dubois and R. Teyssier, *A&A* **482**, L13 (2008), arXiv:0802.0490.
- 390 [42] L. Feretti, G. Giovannini, F. Govoni, and M. Murgia, *A&A Rev.* **20**, 54 (2012),
391 arXiv:1205.1919 [astro-ph.CO].
- 392 [43] E. Churazov, W. Forman, C. Jones, and H. Böhringer, *ApJ* **590**, 225 (2003), astro-
393 ph/0301482.
- 394 [44] J. Aleksić, E. A. Alvarez, L. A. Antonelli, *et al.* (MAGIC Collaboration), *A&A*
395 arXiv:1111.5544.
- 396 [45] P. Kuchar and T. A. Enßlin, *A&A* **529**, A13 (2011).
- 397 [46] V. Vacca, M. Murgia, F. Govoni, L. Feretti, G. Giovannini, R. A. Perley, and G. B. Taylor,
398 *A&A* **540**, A38 (2012), arXiv:1201.4119 [astro-ph.CO].
- 399 [47] M. Ackermann *et al.* (*Fermi*-LAT Collaboration), *Phys. Rev. D* **89**, 042001 (2014).
- 400 [48] M. Ackermann *et al.* (*Fermi*-LAT Collaboration), accepted for publication in *Phys. Rev. Lett.*
401 (2015), arXiv:1503.02641 [astro-ph.HE].
- 402 [49] D. Wouters and P. Brun, *ApJ* **772**, 44 (2013), arXiv:1304.0989 [astro-ph.HE].
- 403 [50] A. Franceschini, G. Rodighiero, and M. Vaccari, *A&A* **487**, 837 (2008), arXiv:0805.1841.
- 404 [51] J. D. Finke, S. Razzaque, and C. D. Dermer, *ApJ* **712**, 238 (2010), arXiv:0905.1115 [astro-
405 ph.HE].
- 406 [52] T. M. Kneiske and H. Dole, *A&A* **515**, A19+ (2010), arXiv:1001.2132 [astro-ph.CO].
- 407 [53] R. C. Gilmore, R. S. Somerville, J. R. Primack, and A. Domínguez, *MNRAS* **422**, 3189
408 (2012), arXiv:1104.0671 [astro-ph.CO].
- 409 [54] Y. Inoue, S. Inoue, M. A. R. Kobayashi, R. Makiya, Y. Niino, and T. Totani, *ApJ* **768**, 197
410 (2013), arXiv:1212.1683.
- 411 [55] R. Bähre, B. Döbrich, J. Dreyling-Eschweiler, *et al.*, *Journal of Instrumentation* **8**, T09001

- 412 (2013), arXiv:1302.5647 [physics.ins-det].
- 413 [56] I. G. Irastorza, F. T. Avignone, G. Cantatore, *et al.*, Journal of Physics Conference Series
414 **460**, 012002 (2013).
- 415 [57] P. Cumani, A. M. Galper, V. Bonvicini, *et al.*, ArXiv e-prints (2015), arXiv:1502.02976
416 [astro-ph.IM].
- 417 [58] M. Actis, G. Agnetta, F. Aharonian, *et al.* (CTA Consortium), Experimental Astronomy **32**,
418 193 (2011), arXiv:1008.3703 [astro-ph.IM].
- 419 [59] B. M. Gaensler, R. Beck, and L. Feretti, New Astronomy Reviews **48**, 1003 (2004), astro-
420 ph/0409100.
- 421 [60] A. Bonafede, F. Vazza, M. Brüggen, T. Akahori, E. Carretti, *et al.*, PoS **AASKA14**, 095
422 (2015), arXiv:1501.00321 [astro-ph.CO].
- 423 [61] M. Meyer and J. Conrad, JCAP **12**, 016 (2014), arXiv:1410.1556 [astro-ph.HE].
- 424 [62] M. Ackermann *et al.* (Fermi-LAT Collaboration), Astrophys.J.Suppl. **203**, 4 (2012),
425 arXiv:1206.1896 [astro-ph.IM].
- 426 [63] A. Mirizzi and D. Montanino, JCAP **12**, 4 (2009), arXiv:0911.0015 [astro-ph.HE].
- 427 [64] A. Mirizzi, G. G. Raffelt, and P. D. Serpico, Phys. Rev. D **76**, 023001 (2007), arXiv:0704.3044.
- 428 [65] A. Dobrynina, A. Kartavtsev, and G. Raffelt, Phys. Rev. D **91**, 083003 (2015),
429 arXiv:1412.4777 [astro-ph.HE].
- 430 [66] D. Horns, L. Maccione, M. Meyer, A. Mirizzi, D. Montanino, and M. Roncadelli, Phys. Rev. D
431 **86**, 075024 (2012), arXiv:1207.0776 [astro-ph.HE].
- 432 [67] N. Bassan, A. Mirizzi, and M. Roncadelli, JCAP **5**, 010 (2010), arXiv:1001.5267 [astro-ph.HE].
- 433 [68] S. S. Wilks, Annals of Mathematical Statistics **9**, 60 (1938).
- 434 [69] G. Cowan, K. Cranmer, E. Gross, and O. Vitells, European Physical Journal C **71**, 1554
435 (2011), arXiv:1007.1727 [physics.data-an].
- 436 [70] M. Ackermann *et al.* (Fermi-LAT Collaboration), Phys. Rev. **D91**, 122002 (2015),
437 arXiv:1506.00013 [astro-ph.HE].
- 438 [71] A. Albert, G. A. Gómez-Vargas, M. Grefe, C. Muñoz, C. Weniger, E. D. Bloom, E. Charles,
439 M. N. Mazziotta, and A. Morselli, JCAP **10**, 023 (2014), arXiv:1406.3430 [astro-ph.HE].
- 440 [72] A. Bonafede, L. Feretti, M. Murgia, F. Govoni, G. Giovannini, D. Dallacasa, K. Dolag, and
441 G. B. Taylor, A&A **513**, A30 (2010), arXiv:1002.0594 [astro-ph.CO] .